Design, synthesis and antimycobacterial activity of benzoxazinone derivatives and open-ring analogues: Preliminary data and computational analysis

Daniele Zampieri[a,*], Maria Grazia Mamolo[a], Julia Filingeri[a], Sara Fortuna[a], Alessandro De Logu[b], Adriana Sanna[c], Davide Zanon[d]

[a] Department of Chemistry and Pharmaceutical Sciences, University of Trieste, P.le Europa 1-Via Giorgeri 1, 34127 Trieste, Italy
[b] Department of Life and Environmental Sciences, University of Cagliari, Via Porcell 4, 09124 Cagliari, Italy
[c] Department of Public Health, Clinical and Molecular Medicine, University of Cagliari, Via Porcell 4, 09124 Cagliari, Italy
[d] Pharmacy and Clinical Pharmacology Department, Institute for Maternal and Child Health IRCCS Burlo Garofolo, Via dell'Istria 65/1, 34137 Trieste, Italy

ARTICLE INFO

Keywords:
Benzoxazinone
Oxoacetamide
Antimycobacterial activity
Molecular dynamics
ADME

ABSTRACT

This study examines in depth benzoxazine nucleus for antimycobacterial property. We synthesized some benzoxazin-2-one and benzoxazin-3-one derivatives, which were tested for activity against a panel of *Mycobacterium tuberculosis* (Mtb) strains, including H37Ra, H37Rv and some resistant strains. Several compounds displayed a high antimycobacterial activity and the three isoniazid analogue derivatives **8a-c** exhibited a MIC range of 0.125–0.250 μg/mL (0.37–0.75 μM) against strain H37Ra, therefore lower than the isoniazid reference drug. Two benzoxazin-2-one derivatives, **1c** and **5j**, together with isoniazid-analogue compound **8a**, also revealed low MIC values against resistant strains and proved highly selective for mycobacterial cells, compared to mammalian Vero cells. To predict whether molecule **8a** is able to interact with the active site of InhA, we docked it into the crystal structure; indeed, during the molecular dynamic simulation the compound never left the protein pocket. The more active compounds were predicted for ADME properties and all proved to be potentially orally active in humans.

More than seventy years have passed since the discovery of streptomycin and sixty-six since isoniazid was synthesized and, despite immense efforts made by the scientific community, tuberculosis (TB) still remains one of the most widespread diseases in the world.

TB is one of the top 10 causes of death worldwide and, in the last few years, it has been the leading cause of death from a single infectious agent, ranking above HIV/AIDS. Diagnosis and successful treatment of people with TB averts millions of deaths each year (an estimated 54 million over the period 2000–2017), but there are still large and persistent gaps in detection and treatment.[1] *Mycobacterium tuberculosis* (Mtb) is the causative agent of the disease, for which treatment regimens are both lengthy and toxic. Furthermore, the spread of multidrug-resistant strains (MDR) worsen the course of disease. In spite of some new drugs, such as Bedaquiline and Delamanid, there is a pressing need for new chemical entities with a clear mechanism of action and a selective profile against Mtb, in particular against resistant strains.

Currently there are several mycobacterial targets such as 2-*trans*-enoyl-ACP (CoA) reductase (InhA),[2] alanine-racemase,[3] metioninaminopeptidase (MetAP),[4] isocitrate lyase (ICL),[5] menaquinone-B (MenB),[6] decaprenyl-phosphoryl-β-D-ribose oxidase (DprE1)[7] and others, most of which act on the mycobacterial cell-wall.

Benzoxazine moiety is present in several structures endowed with various activities, such as antiallergics,[8] antimicrobials,[9] antimycobacterials[6] and antifungals.[10] The antimycobacterial activity of some benzoxazin-2-one compounds is due to the inhibition of MenB, a synthetic pathway involving menaquinone, one of the essential

Abbreviations: ADME, absorption metabolism distribution excretion; CC50, cytotoxic concentration 50%; DprE1, decaprenyl-phosphoryl-β-D-ribose oxidase; HBA, h-bond acceptor; HBD, h-bond donor; IC50, inhibition concentration 50%; INH, isoniazid; InhA, 2-*trans*-enoyl-ACP (CoA) reductase; MD, molecular dynamics; MDR, multidrug resistant strains; Men-B, menaquinone-B; MetAP, metioninaminopeptidase; MIC, minimum inhibitory concentration; MM-PBSA, molecular mechanics Poisson-Boltzmann surface area; Mtb, Mycobacterium tuberculosis; MTT, 3-(4,5-dimethylthiazol-2-yl)-2,5-diphenyltetrazolium bromide; MW, molecular weight; NAD, nicotinamide adenine dinucleotide; NADH, nicotinamide adenine dinucleotide reduced form; RMSD, root mean squared deviation; RMSF, root mean squared fluctuation; SASA, solvent accessible surface area; TB, tuberculosis

* Corresponding author.
E-mail address: dzampieri@units.it (D. Zampieri).

Accepted 16 July 2019

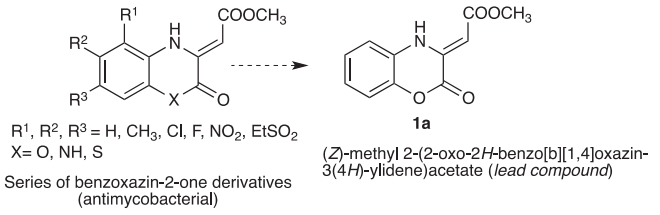

Fig. 1. Structure of benzoxazin-2-one reference compound **1a**.

components of the electron transport chain in many pathogens including mycobacteria (in humans this role is played by ubiquinone). This is the starting point of the current work, which focuses on exploring the chemical significance of the benzoxazine nucleus for antimycobacterial activity.

(*Z*)-methyl-2-(2-oxo-2*H*-benzo[b][1,4]oxazin-3(4*H*)-ylidene)acetate **1a** was the lead compound of a series of derivatives selected through HTPS by Li and coworkers.[6] The authors studied the effect of the substitution on the aromatic portion of the benzoxazin-2-one core with different groups such as Cl-, F-, CH_3- NO_2-, both on antimycobacterial activity and on enzymatic inhibition (Fig. 1). In addition to the unsubstituted compound, which exhibited the best value of enzymatic inhibition (IC_{50} = 10 μM) and MIC value 0.64 μg/mL (2.9 μM), the work highlighted the importance of the substitution with a halogenated atom (F and Cl) on the aromatic ring of the benzoxazin-2-one core, in particular they found the same antimycobacterial activity for the 7-Cl substituted derivative (**1c**) (MIC = 0.63 μg/mL) and a decreased activity when the substituent was in position C-6 (**1b**) (MIC = 5 μg/mL) and a slight increase of the enzymatic inhibition values (IC_{50} = 46.3 and 35.7 μM respectively).

In order to assess the relevance of the chemical space around the oxazine core and its importance for antimycobacterial activity, we planned to synthesize reference compounds **1a-c** and a second generation of benzoxazin-2-one derivatives, and test them against several mycobacterial strains. The aim was to evaluate modifications such as the introduction of bulky substituents (**2a,b**), or a heterocycle ring (**2c**) (Fig. 2a), as well as reductions of the exocyclic double bond, **3** and the oxazinone carbonyl group, **4** of the original lead compound **1a**, as depicted in Fig. 2b. Furthermore, we replaced the original ester functional group with several aroyl groups, **5a-l** (Fig. 2c).

Subsequently, we decided to synthesize the isoster (*E*)-methyl-2-(3-oxo-3,4-dihydro-2*H*-benzo[b][1,4]oxazin-2-ylidene)acetate **6** and some analogues substituted both on nitrogen atom and on vinylic function, **7a-f** and three INH-analogues **8a-c**, fusing the (substituted)benzoxazine-2,3-dione core with INH. Unexpectedly, the reaction to obtain the benzoxazin-3-one-INH hybrids led to an open-ring form, corresponding

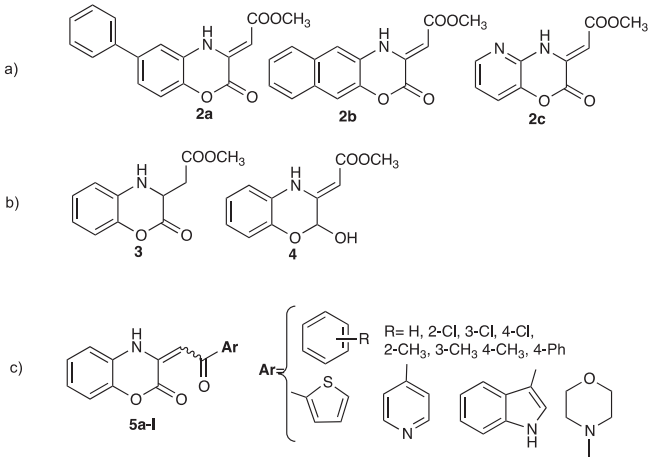

Fig. 2. (a) Structure of benzoxazin-2-one compounds **2a-c**; (b) Structure of reduced compounds **3** and **4**; (c) Structure of title compounds **5a-l**.

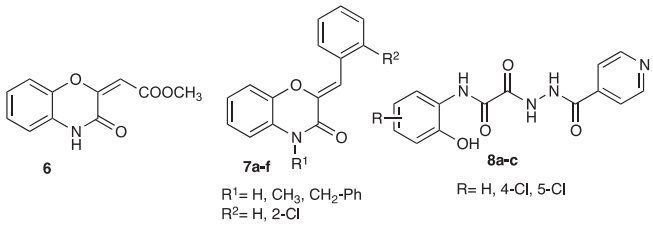

Fig. 3. Structure of the isosteric benzoxazin-3-one derivatives **6** and **7a-f** and oxoacetamide-INH compounds **8a-c**.

to the N-(2-hydroxyphenyl)-2-(2-isonicotinoylhydrazinyl)-2-oxoacetamide **8a** and its chloro-substituted analogues **8b,c** (Fig. 3, Fig. SI 1 and Scheme 1).

The synthetic route to prepare all the benzoxazinone derivatives is depicted in Scheme 1.

The lead compound (*Z*)-methyl 2-(2-oxo-2*H*-benzo[b][1,4]oxazin-3(4*H*)-ylidene)acetate **1a** and its halogenated analogues **1b,c**, were obtained from 2-aminophenol, 4-chloroaminophenol or 5-chloroaminophenol and dimethyl but-2-ynedioate; starting from 3-amino-[1,1′-biphenyl]-4-ol,3-aminonaphtalen-2-ol and 2,4-diaminophenol, the same synthetic pathway led to analogue compounds **2a-c**. All these derivatives are in enamine form (*Z* configuration) due to the stabilization of the intramolecular H-bond between oxazine NH group and exocyclic carbonyl ester (Fig. 4); the treatment of compound **1a** with H_2/Pd-$C_{10\%}$ or $NaBH_4$ yield the corresponding reduced compounds **3** and **4**, respectively. Series **5a-l** was synthesized by Claisen condensation between several arylethanones and diethyl oxalate in basic media (NaOEt), and then the substituted butenoate intermediates **9a-l** were cyclized with 2-aminophenol in acetic acid. The synthesis of (*E*)-methyl 2-(3-oxo-3,4-dihydro-2*H*-benzo[b][1,4]oxazin-2-ylidene)acetate **6** was carried out via 2-step reaction involving the formation of intermediate (*Z*)-4-((2-hydroxyphenyl)amino)-2-(methoxycarbonyl)-4-oxobut-2-enoic acid **10** obtained by the reaction of 2-aminophenol and 3-bromofuran-2,5-dione in 1,4-dioxane at room temperature; the subsequent cyclization with triethylamine at reflux temperature provided the desired product **6** in *E* configuration (94%). Derivatives **7a-f** were synthesized by treating 2*H*-benzo[b][1,4]oxazin-3(4*H*)-one **11** with benzaldehyde (**7a**), or 2-chlorobenzaldehyde (**7b**) in the presence of sodium methoxide in DMF at reflux temperature and subsequently *N*-alkylated with methyl iodide (**7c,d**) or benzyl chloride (**7e,f**). All the derivatives synthesized were in *Z* configuration (Fig. 4) due to the steric hindrance of the substituted phenyl moiety on the cyclic carbonyl group. The INH-analogue molecules **8a-c** were obtained by treating isoniazid (INH) with 2*H*-benzo[b][1,4]oxazine-2,3(4*H*)-dione intermediate **12a** and the substituted 6-chloro **12b** and 7-chloro **12c** intermediates, respectively, with a typical Schiff reaction to yield the oxoacetamide compounds **8a-c**, instead of the expected benzoxazin-3-one-INH hybrids.

Lead compound (*Z*)-methyl-2-(2-oxo-2*H*-benzo[b][1,4]oxazin-3(4*H*)-ylidene)acetate **1a**, and its halogenated analogues **1b,c**, revealed MIC values of 4 μg/mL for **1a**, whereas values of 16 μg/mL and 2 μg/mL were found for **1b** and **1c**, respectively. The bulky benzoxazin-2-one derivatives **2a,b**, as well as the heterocycle derivative pyridoxazin-2-one **2c**, were devoid of antimycobacterial activity (MIC > 64 μg/mL). These findings confirm that the increased steric hindrance (**2a,b**), or the presence of a protonable atom such as nitrogen (**2c**) into the aromatic portion of benzoxazine core, worsens the antimycobacterial activity.

Investigating more thoroughly the original benzoxazin-2-one scaffold (**1a**), the corresponding reduced compounds **3** and **4** provided interesting information. Infact, the title compound **3**, bearing a reduced exocyclic double bond, showed a two-fold higher MIC value 8 μg/mL compared to the lead compound **1a**, while derivative **4**, having a hydroxyl group in place of the carbonyl group in position 2, proved to be a weak Mtb inhibitor (MIC = 64 μg/mL). The latter data indicate the

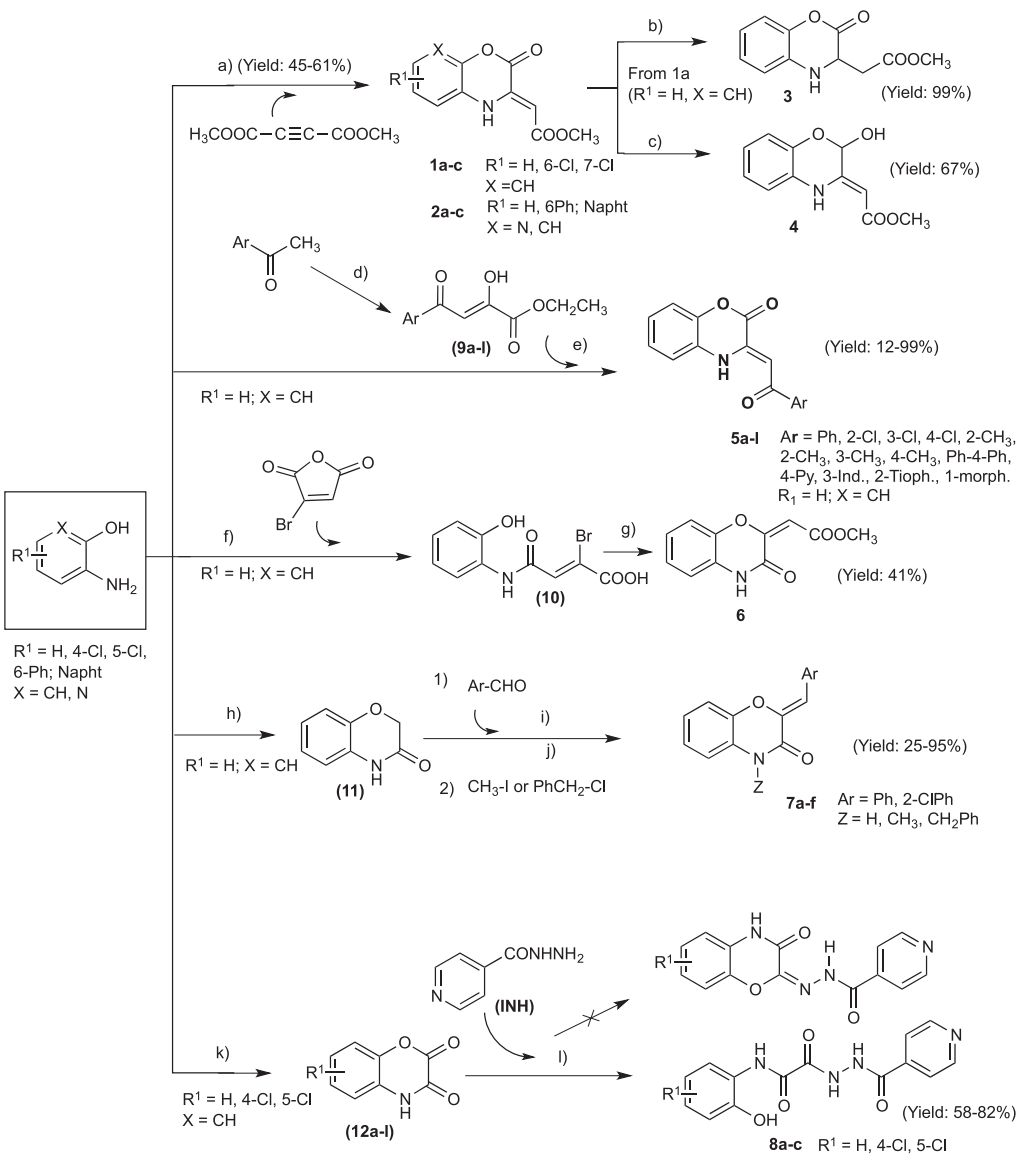

Reagents and conditions: a) MeOH, rt, N_2; b) EtOH, H_2-Pd/C, rt; c) MeOH, $NaBH_4$,rt; d) EtOH, NaOEt, rt; e) AcOH, reflux; f) 1,4-Dioxane, rt; g) MeOH, Et_3N, reflux; h) CH_2Cl_2, K_2CO_3, Bromoacetyl bromide, 0°C then rt; i) DMF, NaOMe, reflux; j) Acetone, K_2CO_3/KI cat, reflux; k) Toluene, Oxalyl chloride, reflux; l) EtOH, reflux.

Scheme 1. Synthetic route of title compounds **1**–**8**.

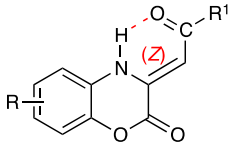

Fig. 4. H-bond involved in benzoxazin-2-one compounds.

necessary presence of an H-bond acceptor group at position C2 (Fig. 2b) of the benzoxazin-2-one core, instead of an H-donor group (OH), while the increased mobility of the ester side chain due to the saturation of the double bond seems to have only a slight effect on the anti-mycobacterial activity. Series **5a-l** gave the best results of the benzoxazin-2-one series, in terms of inhibition of mycobacteria growth, in fact all the compounds proved to be more active, with MIC range of 2–4 μg/mL, than lead compound **1a**. In particular, heterocyclic substituted derivatives **5j-l** were found to be the most active molecules with MIC of 2 μg/mL. The slight difference in terms of MIC values within the series highlights the importance of the aromatic, bulky substitution in the side chain of the benzoxazin-2-one scaffold in place of an exclusively ester functional group and, particularly, the significance of the heterocyclic substitution. This information differs slightly from previous results in terms of antimycobacterial activity of a small series of substituted (*Z*)-3-[2-(2-chlorophenyl)-2-oxoetylidene]-3,4-dihydro-2*H*-benzo[b][1,4]oxazin-2-one compounds[6]; in fact the authors found that all the series proved to be less active than lead ester compound **1a**, against Mtb.

Curiously, isoster benzoxazin-3-one derivatives **6** and **7a-f** are weak inhibitors of Mtb, revealing MIC value of 64 μg/mL and contradicting the bioisosterism principle. INH analogue derivatives **8a-c** were also tested against Mtb H37Ra and the data obtained showed a MIC range of 0.125–0.250 μg/mL, with the best inhibition value for unsubstituted and 5-chloro-substituted derivatives **8a,b** (MIC = 0.125 μg/mL or 0.37 μM), more than twice as powerful of INH in terms of micro molar MIC (0.125 μg/mL or 0.91 μM), thus proving to be the best candidates of the entire series.

Conversely to what happens with series **1a,c**, where the position of

Table 1
Antimycobacterial activity, MIC μg/mL (μM), of title compounds **1–8** against Mtb strain H37Ra and cytotoxicity of compounds **1a-c**, **3**, **5a-l** and **8a-c**, in comparison with reference compounds INH against Vero cell line.

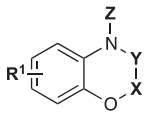

1-7

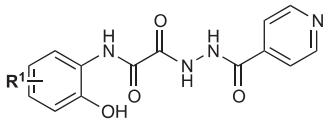

8a-c

Cpd	X	Y	R^1	Z	*M. tuberculosis* ATCC25197 H37Ra		
					MIC μg/mL (μM)	CC_{50} μg/mL (μM)	S.I.[a]
1a	C=O	C=CH-$COOCH_3$	H	H	4 (18)	500 (> 2281)	> 125
1b	C=O	C=CH-$COOCH_3$	6-Cl	H	16 (63)	413 (1628)	26
1c	C=O	C=CH-$COOCH_3$	7-Cl	H	2 (7.9)	405 (1596)	202
2a	C=O	C=CH-$COOCH_3$	6-Ph	H	64 (145)	nt[b]	nt
2b	C=O	C=CH-$COOCH_3$	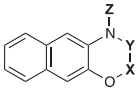	H	> 64 (> 238)	nt	nt
2c	C=O	C=CH-$COOCH_3$		H	> 64 (> 217)	nt	nt
3	C=O	CH-CH_2-$COOCH_3$	H	H	8 (36)	342 (1546)	43
4	CH-OH	C=CH-$COOCH_3$	H	H	64 (289)	nt	nt
5a	C=O	C=CHCO-Ph	H	H	4 (15)	> 250 (> 942)[c]	> 62
5b	C=O	C=CHCO-2-ClPh	H	H	4 (13)	472 (1573)	118
5c	C=O	C=CHCO-3-ClPh	H	H	4 (13)	482 (1606)	120
5d	C=O	C=CHCO-4-ClPh	H	H	4 (13)	375 (1251)	94
5e	C=O	C=CH-CO-*o*-tolyl	H	H	4 (14)	> 500 (> 1790)	> 125
5f	C=O	C=CH-CO-*m*-tolyl	H	H	4 (14)	> 500 (> 1790)	> 125
5g	C=O	C=CH-CO-*p*-tolyl	H	H	4 (14)	461 (1650)	115
5h	C=O	C=CH-CO-4-PhPh	H	H	4 (12)	> 125 (> 366)[c]	> 30
5i	C=O	C=CH-CO-4-Pyr	H	H	4 (15)	> 500 (> 1878)	> 125
5j	C=O	C=CH-CO-3-Indol	H	H	2 (6.5)	> 500 (> 1643)	> 250
5k	C=O	C=CH-CO-2-Thiof	H	H	2 (7.3)	> 500 (> 1845)	> 250
5l	C=O	C=CH-CO-1-Morph	H	H	2 (7.3)	310 (1138)	155
6	C=CH-$COOCH_3$	C=O	H	H	64 (291)	nt	nt
7a	C=CH-Ph	C=O	H	H	64 (270)	nt	nt
7b	C=CH-2ClPh	C=O	H	H	64 (238)	nt	nt
7c	C=CH-Ph	C=O	H	CH_3	64 (127)	nt	nt
7d	C=CH-2ClPh	C=O	H	CH_3	64 (224)	nt	nt
7e	C=CH-Ph	C=O	H	CH_2-Ph	64 (196)	nt	nt
7f	C=CH-2ClPh	C=O	H	CH_2-Ph	64 (177)	nt	nt
8a	–	–	H	–	0.125 (0.42)	423 (1409)	3384
8b	–	–	5-Cl	–	0.125 (0.37)	402 (1201)	3316
8c	–	–	4-Cl	–	0.250 (0.75)	390 (1165)	1560
INH	–	–	–	–	0.125 (0.91)	> 1000 (> 7300)	> 8000

[a] CC_{50}/MIC H37Ra;
[b] not tested;
[c] Maximum solubility (DMSO) beyond which it precipitates in the medium.

the electron-withdrawing substituent on the benzoxazine aromatic core markedly influences antimycobacterial activity, with oxoacetamide-INH derivatives **8a,c**, this pattern is less significant.

The most interesting compounds were chosen to evaluate their *in vitro* cytotoxicity in the mammalian Vero cell line using the MTT colorimetric assay. The results are reported both as CC_{50} and Selectivity Index, S.I. (Table 1). The S.I. is an evaluation of the selectivity of the molecules between eukaryotic and mycobacterial cells, thus a value of safety of our title compounds. According to a study of Hartkoorn and coworkers[11] on TB drug susceptibility, antimycobacterial activity is considered to be specific when the selectivity index is > 10 and our compounds turned out to be much more selective than required. In fact, the collected data are in the range of 125–500 μg/mL in terms of CC_{50} and a selectivity index of 26–3384. Interestingly, the most active molecules against strain H37Ra, **1a-c** and **8a-c**, also proved to be the safest with CC_{50} ranging from 390 to 500 μg/mL.

Reference compounds **1a-c** and the most active molecules of the two series, heterocyclic derivatives **5j-l** and the INH analogue derivatives **8a-c**, were also tested against Mtb strain H37Rv and several resistant strains as reported in Table 2.

All the compounds displayed the same previous trend against H37Rv with MIC range of 1–8 μg/mL with the best values for the three INH-analogue molecules **8a-c** (1 μg/mL), while all the derivatives proved to be virtually ineffective against the INH-resistant strain. The most interesting results were obtained against the pyrazinamide-, rifampicin- and streptomycin-resistant strains. Indeed, all the compounds exhibited a marked antimycobacterial activity, with MIC range of 1–16 μg/mL. The best results were obtained by 7-chloro- and indolyl-derivatives of the benzoxazine-2-one series, **1c** and **5j**, both with MIC values of 1 μg/mL.

The X-ray structure of the enzyme inhibitor complex has been known for two decades (1ZID)[12] showing the InhA bound to an INH-

Table 2
Antimycobacterial activity, MIC μg/mL (μM) of compounds **1a-c**, **5j-l** and **8a-c** in comparison with reference compound isoniazid (INH) against strain H37Rv and four resistant strains of *M. tuberculosis*.

Cpd	MIC μg/mL (μM)				
	ATCC 27294 H37Rv	ATCC 35822 INH-R[a]	ATCC 35828 Pyr-R[b]	ATCC 35838 Rifa-R[c]	ATCC 35820 Str-R[d]
1a	1 (4.5)	> 32 (> 146)	1 (4.5)	2 (9.1)	1 (4.5)
1b	8 (31)	> 32 (> 126)	8 (31)	16 (63)	16 (63)
1c	1 (3.9)	> 32 (> 126)	1 (3.9)	1 (3.9)	1 (3.9)
5j	1 (3.3)	> 32 (> 105)	1 (3.3)	1 (3.3)	1 (3.3)
5k	4 (14.7)	32 (118)	4 (14.7)	4 (14.7)	4 (14.7)
5l	2 (7.3)	> 32 (> 117)	1 (3.6)	2 (7.3)	2 (7.3)
8a	1 (3.3)	> 32 (> 106)	2 (6.7)	1 (3.3)	8 (26.7)
8b	1 (3.1)	> 32 (> 96)	4 (12.0)	4 (12.0)	8 (24.0)
8c	1 (3.1)	> 32 (> 96)	4 (12.0)	4 (12.0)	8 (24.0)
INH	0.25 (1.8)	> 32 (> 233)	0.25 (1.8)	0.25 (1.8)	0.25 (1.8)

[a] Isoniazid-resistant strain;
[b] Pyrazinamide-resistant strain;
[c] Rifampicin-resistant strain;
[d] Streptomycin-resistant strain.

adduct. INH is in fact activated forming an acyl pyridine adduct with NAD (or INH-NAD). Further structures for InhA bound to an INH-adduct include 2PR2[13] with INH-NADP, 2IDZ[14] with NADH-INH and 2NV6, an isoniazid resistant S94A mutant with INH-NAD adduct.[15] By overlapping them the INH units closely overlay in the protein pocket. It is clear from the crystal structures that there are two possible positions for conjugated rings: one occupied by the INH and the other one occupied by the adenine.

To predict whether one of the most interesting compounds of our series, the INH-analogue **8a**, is able to interact with the active site of the protein pocket, we docked it into the site, and starting from the resulting configuration we ran 250 ns molecular dynamics (MD) simulation in full water solvent.

We chose to work with the wild type 2 Å resolution 2IDZ.[14] We first tested our method by removing the highly flexible ligand and dock it back into the protein pocket. With the genetic algorithm and simulated annealing of AutoDock it was not possible to obtain a molecule with the expected orientation, a problem not encountered with AutoDock Vina which led to a first ranked conformation with RMSD 0.72 Å compared to the crystal structure and a predicted binding affinity of −12.4 kcal/mol (Fig. SI 2).

We then docked compound **8a** in the same pocket obtaining first ranked conformation with a predicted binding affinity of −8.6 kcal/mol (Fig. SI 5a). Among the other top ranked complexes, we identified 4 other similar conformations with RMSD < 1.30 Å in comparison with the first one and with binding energies between −8.5 kcal/mol and −8.4 kcal/mol (Fig. SI 3). The remaining poses, though occupying the same site, are flipped compared to the others, as the hydroxyphenyl group occupies the position of the isonicotinoyl group and vice versa.

In the top-ranking binding pose (Fig. SI 4a), the isonicotinoyl group occupies the same adenine position of the original binder (Fig. SI 4b). All the amino acids that held compound **8a** in place but one were also found to interact with the original ligand. Both molecules were held in place thanks to a hydrogen bond with Ile21, and with compound **8a** forming an additional hydrogen bond with Gly96.

We then performed 250 ns MD simulation on the complex formed by InhA and the top ranked binding pose of compound **8a**. The ligand topologies built with ATB[16] led to a minimized molecular geometry with a RMSD of 0.1721 Å compared to the semi-empirical quantum chemistry minimization, thus validating the generated force field parameters. Along the MD trajectory we re-scored the complex with the same scoring function used for generating the docked poses (Fig. SI 5b).

During the simulation, the VINA energy values reached −12.8 kcal/mol. The lowest energy conformation corresponded to a shift in the location of compound **8a** in the protein pocket associated with a clear variation in protein conformation (Fig. SI 5c) and the presence of an intermolecular hydrogen bond, and two hydrogen bonds with the protein one with Ser 94 and one with Gly 96 (Fig. SI 4c).

The system equilibrates after 120 ns at which point compound **8a** assumes a new conformation. This can be appreciated by looking at the root mean square deviation (RMSD) of compound **8a** calculated, compared to a fixed protein backbone (Fig. 5a): at the beginning of the simulation the compound migrated to a new position, and further rearranged. The change in compound configuration seems not associated

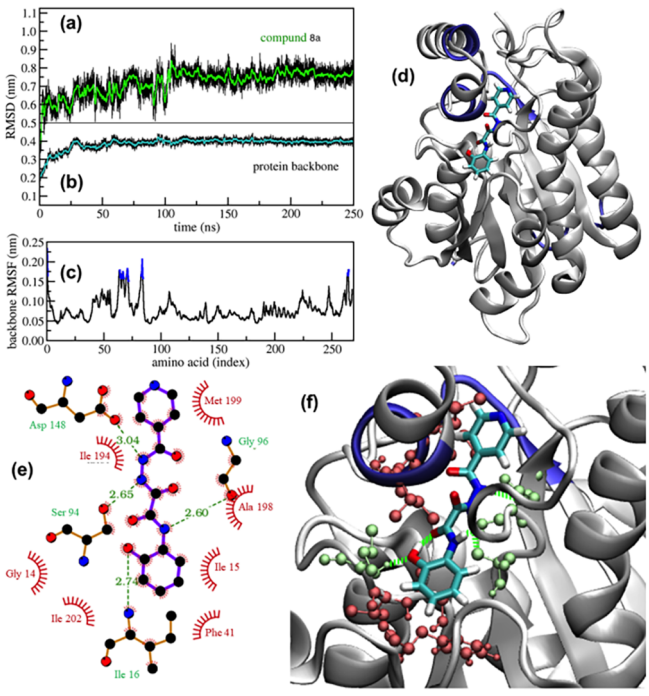

Fig. 5. Trajectories analysis: (a) compound **8a** RMSD in the frame of the protein backbone (black) and its running average (green); (b) protein backbone RMSD (black) and its running average (cyan); (c) protein backbone RMSF calculated over the last 100 ns (black) with values above 0.15 nm highlighted in blue; (d) simulation snapshot at t = 193.9 ns where protein residues with backbone RMSF larger than 0.15 nm are highlighted in blue; (e) schematic diagram of the interaction between InhA and compound **8a** at t = 193.9 ns (f) close ups on compound **8a** at t = 193.9 ns. In (e-f) protein residues interacting with the target by van der Waals interactions are highlighted in red/orange, while those forming hydrogen bonds are green. Hydrogen bonds distances measured in nm are also indicated.

with major protein rearrangements, as indicated by the little fluctuations observed in the protein backbone RMSD (Fig. 5b). Also, the protein reaches equilibrium at 120 ns. Over the last 100 ns of the MD simulation, the backbone root mean squared fluctuation (RMSF, Fig. 5c) indicates that only few residues were found above 0.15 nm with the majority not reaching 0.10 nm. In the same time interval, the average VINA score, calculated over the data of Fig. 5b, equals −10.3 kcal/mol.

To understand the details of the equilibrium configuration we looked at the lowest energy pose found along the last 100 ns of the MD trajectory. That is at t = 193.9 ns with a VINA score of −12.4 kcal/mol (Fig. SI 5b). In this configuration compound **8a** reached a steady state in the protein pocket (Fig. 5d). The compound was held in place thanks to four hydrogen bonds (Fig. 5e), while one intermolecular hydrogen bond kept the molecule in a fixed configuration. Six protein side chains contribute to the binding, and a flexible loop was capable of adapting to the ligand conformation and instant position in the pocket (Fig. 5f), resulting in a concerted movement that enabled binding interactions to maintain their strength.

We finally performed a MM-PBSA analysis to clarify the nature of the energetic contributions to the protein/compound interaction. Using the MM-PBSA method, binding free energy (ΔG) was calculated as follows[17]:

$$\Delta G = \Delta E - \Delta S + \Delta G_{solv} \text{ with } \Delta E = E_{vdW} + E_{el} \text{ and } \Delta G_{solv} = \Delta G_{polar} + \Delta G_{apolar}$$

where E_{vdW} is the van der Waals energy contribution and E_{el} is the electrostatic energy contribution to the ligand/protein binding energy ΔE, T is the temperature, ΔS the variation in entropy between unbound and bound state, and ΔG_{solv} the desolvation free energy with its polar ΔG_{polar} and apolar ΔG_{apolar} contributions (the latter here calculated with the solvent accessible surface area, SASA, method). As we neglect here the entropic contribution, we call the term $\Delta E + \Delta G_{solv}$ simply total binding energy.

The MM-PBSA analysis (Fig. 6) revealed that both van der Waals and electrostatic contributions kept compound **8a** in place (Fig. 6). Amino acid energetic contributions on average larger than ± 0.5 kcal/mol (Fig. 6b) were associated with Ile 202, Phe 149, Glu 219, Gly 96, Ile 194, Phe 97, Ile 95, Met 199, Pro 156, with only Asp 148 clearly opposing the binding (details in SI, Fig. SI 6).

We computationally verified whether the identified compound **8a** was capable of fitting in the protein pocket. The docking result led to an estimated score of −8.6 kcal/mol corresponding to K_d 0.50 μM at room temperature, a value that after 150 ns MD simulation reduced to an average of −10.3 kcal/mol (K_d = 28 nM). Analysis of the MD trajectory revealed that compound **8a** is held in its binding site by four hydrogen bonds (Fig. 5e), while Asp 148 opposes binding due to weak electrostatic and van der Waals not capable of counteracting the unfavorable desolvation. This was also observed in the MM-PBSA contributions to the total binding energy (Fig. 6a).

All the derivatives endowed with antimycobacterial activity (MIC < 64 μg/mL) were evaluated *in silico* (Table SI1) for prediction of drug likeness properties,[18] using the most common pharmacokinetic parameters, on the basis of the extended version of Lipinski's rule of five (RO5).[19] The RO5 extended criterion means that an orally active drug should not violate more than one of the following requirements: MW ≤ 500; HBA and HBD (related to membrane permeability) ≤ 10 and ≤ 5, respectively; logP and logS (related to intestinal absorption) ≤ 5; PSA ≤ 140 Å. All the evaluated compounds, in comparison with lead compound **1a** and INH as reference standard, exhibited good drug-likeness properties, as all the values fell within the ranges of RO5.

In conclusion, this study builds on a previous exploratory study investigating the oxazinone core for antimycobacterial activity started by Li and coworkers.[6] We synthesized different series of compounds both with benzoxazin-2-one (**2a-c**, **3**, **4**, and **5a-l**) and benzoxazin-3-one (**6**, **7a-f**) scaffolds. Also, we synthesized three new open-ring analogues, such as oxoacetamide derivatives, presenting isoniazid moiety (**8a-c**). All the title compounds were evaluated against several mycobacterial

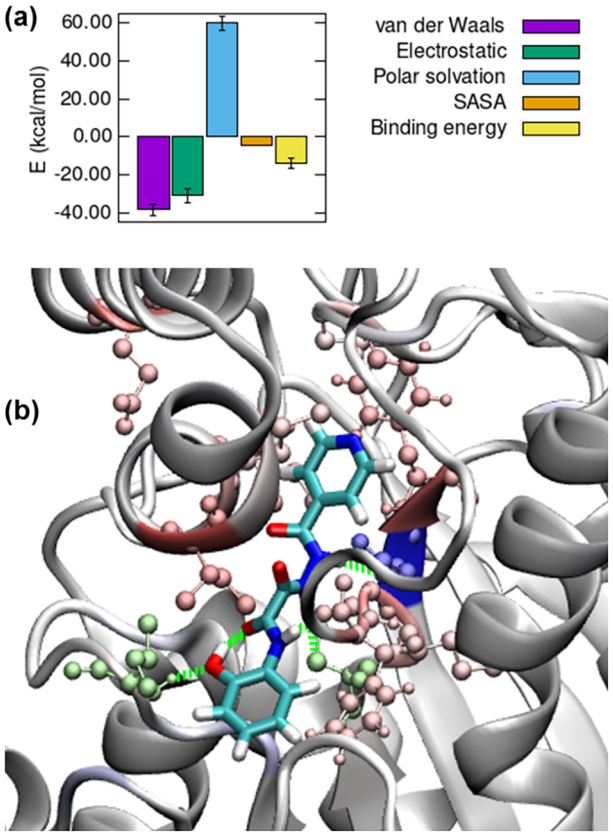

Fig. 6. (a) Contributions to the total binding energy averaged over 150–250 ns time interval. (b) close ups on compound **8a** with highlighted amino acids with positive (shades of red) and negative (shades of blue) contribution to the binding energy larger than ± 0.5 kcal/mol, snapshot taken at t = 193.9 ns. All the data refers to 150–250 ns time interval.

strains, including strain H37Ra, H37Rv and four strains resistant to first-line drugs used for TB treatment. One of the most interesting compounds found was derivative **8a**, a combined molecule of N-(2-hydroxypheny)-2-oxoacetamide fragment and INH. In order to predict whether compound **8a** was able to interact with the active site of the 2-*trans*-enoyl-ACP (CoA) reductase (InhA), the isoniazid biological target, we docked it into the crystal structure, and then we performed 250 ns MD simulation in full water solvent. During the simulation, the compound never left the protein pocket, proving strong interactions with the active site of the enzyme. However, further study will be required to fully characterize the new system.

The data obtained revealed that most of our benzoxazine derivatives, in particular the benzoxazin-2-one series, are very selective for Mtb confirming that their biological target (MenB) is specific of the mycobacterial cell (high CC_{50} and S.I. values towards eukaryotic Vero cells) and that the benzoxazin-2-one moiety is a key scaffold for antimycobacterial activity. Any kind of modification on the aromatic fragment of the benzoxazin-2-one ring seems to detriment the activity, as well as the isosteric benzoxazin-3-one and some of its derivatives. On the other hand, structural modification in the side chain of the benzoxazine core, can lead to compounds gifted with marked antimycobacterial activity, also against resistant strains. Finally, the oxoacetamide-INH molecules proved to be even more active than INH against strain H37Ra and showed a comparable inhibition grade towards several resistant strains. An *in silico* prediction of the common pharmacokinetics and physiochemical parameters (ADME), revealed that the most active compounds could be potentially orally active in humans.

Although still preliminary and requiring further studies, these findings suggest that oxoacetamide-INH molecules could be considered a new

series of INH analogue derivatives with improved antimycobacterial activity and a potentially promising new class of antitubercular agents.

Acknowledgments

The financial support of FRA 2016 Research Fund University of Trieste-Italy (owner: Dr. Daniele Zampieri), is gratefully acknowledged. We also acknowledge the CINECA Awards N. HP10C70TG1, 2018, for the availability of high performance computing resources and support. The authors would like to thank Dr. Fabio Hollan (Dep. Of Chemistry and Pharmaceutical Sciences-Univ. of Trieste) for MS data.

References

1. WHO TB report 2018.
2. Vilcheze C, Morbidoni HR, Weisbrod TR, et al. Inactivation of the inhA-encoded fatty acid synthase II (FASII) enoyl-acyl carrier protein reductase induces accumulation of the FASI end products and cell lysis. *Bacteriology.* 2000;182:4059–4067.
3. Milligan DL, Tran SL, Strych U, Cook GM, Krause KL. The alanine racemase of Mycobacterium smegmatis is essential for growth in the absence of D-alanine. *J Bacteriol.* 2007;189:8381–8386.
4. Olaleye O, Raghunand TR, Bhat S, et al. Methionine aminopeptidases from Mycobacterium tuberculosis as novel antimycobacterial targets. *Chem Biol.* 2010;17:86–97.
5. Krátký M, Vinsová J, Novotná E, et al. Salicylanilide derivatives block Mycobacterium tuberculosis through inhibition of isocitrate lyase and methionine aminopeptidase. *Tuberculosis.* 2012;92:434–439.
6. Li X, Liu N, Zhang H, Knudson SE, Slayden RA, Tonge PJ. Synthesis and SAR studies of 1,4-benzoxazine MenB inhibitors: novel antibacterial agents against Mycobacterium tuberculosis. *Bioorg Med Chem Lett.* 2010;20:6306–6309.
7. Makarov V, et al. Benzothiazinones Kill Mycobacterium tuberculosis by blocking Arabinan synthesis. *Science.* 2009;324:801–804.
8. Loev B, Jones H, Brown RE, et al. [1,4]benzoxazin-2,3-dione as antiallergic agents. *J Med Chem.* 1985;28:24–27.
9. Babenysheva A, Lisovskaya N, Belevich I, Lisovenko N. Synthesis and antimicrobial activity of substituted benzoxazines and quinoxalines. *Pharm Chem J.* 2006;40:611–613.
10. Fringuelli R, Giacche N, Milanese L, et al. Bulky 1,4-benzoxazine derivatives with antifungal activity. *Bioorg Med Chem.* 2009;17:3838–3846.
11. Hartkoorn RC, Chandler B, Owen A, et al. Differential drug susceptibility of intracellular and extracellular tuberculosis and the impact of P-glycoprotein. *Tuberculosis.* 2007;87:248–255.
12. Rozwarski DA, Grant GA, Barton DHR, Jacobs Jr WR, Sacchettini JC. Modification of the NADH of the isoniazid target (InhA) from Mycobacterium tuberculosis. *Science.* 1998;279:98–102.
13. Argyrou A, Vetting MW, Blanchard JS. New insight into the mechanism of action of and resistance to isoniazid: interaction of Mycobacterium tuberculosis enoyl-ACP reductase with INH-NADP. *J Am Chem Soc.* 2007;129:9582–9583.
14. Dias MVB, Vasconcelos IB, Prado AMX, et al. Crystallographic studies on the binding of isonicotinyl-NAD adduct to wild-type and isoniazid resistant 2-*trans*-enoyl-ACP (CoA) reductase from Mycobacterium tuberculosis. *J Struct Biol.* 2007;159:369–380.
15. Vilchèze C, Wang F, Arai M, et al. Transfer of a point mutation in Mycobacterium tuberculosis inhA resolves the target of isoniazid. *Nat Med.* 2006;12:1027–1029.
16. Malde AK, Zuo L, Breeze M, et al. Automated force field topology builder (ATB) and repository: version 1.0. *J Chem Theory Comp.* 2011;7:4026–4037.
17. Kumari R, Lynn AM. g_mmpbs-a GROMACS tool for high-throughput MM-PBSA calculations. *J Chem Inf Model.* 2014;54:1951–1962.
18. Daina A, Michielin O, Zoete V. SwissADME: a free web tool to evaluate pharmacokinetics, drug-likeness and medicinal chemistry friendliness of small molecules. *Sci Rep.* 2017;7:42717.
19. Lipinski CA. Lead- and drug-like compounds: the rule-of-five revolution. *Drug Discovery Today, Technol.* 2004;1:337–341.